Mass Estimation Relationship for Conceptual Design of Blended-Wing-Body Cabin with Advanced Structures

James Joseph[1], David J. Kinney[2], and Joseph A. Garcia[3]

NASA Ames Research Center, Moffett Field, CA, USA

Jeffrey V. Bowles[4]

Ames Research Associate, Moffett Field, CA, USA

Blended-Wing-Body (BWB) aircraft concepts achieve higher lift-to-drag ratios (L/D) than conventional tube and wing aircraft due to aerodynamic shaping of the non-circular pressure vessel that is made feasible using advanced composite technologies such as Pultruded Rod Stitched Efficient Unitized Structure (PRSEUS). Due to the relatively new nature of the BWB configuration, sufficient historical data is not readily available for conceptual aircraft designers to base their structural weight estimations on, especially for estimating weights of the pressurized cabin center body. This paper describes a general parametric Mass Estimation Relationship (MER) based on high fidelity Finite Element Analysis (FEA) using PRSEUS for conceptual weight estimation of a BWB pressurized cabin structure that includes cabin area, center body sweep, fineness ratio, span ratio, and take-off gross weight as parametric design variables.

I. Nomenclature

BWB	=	Blended-Wing-Body
MER	=	Mass Estimation Relationship
L/D	=	Lift to Drag ratio
L	=	Lift
D	=	Drag
T&W	=	Tube & Wing
PRSEUS	=	Pultruded Rod Stitched Efficient Unitized Structure
FEA	=	Finite Element Analysis
TOGW	=	Take Off Gross Weight
FEM	=	Finite Element Model
GASP	=	General Aircraft Synthesis Program
FLOPS	=	FLight OPtimization System
t/c	=	Thickness to Chord ratio
RHS	=	Right Hand Side
LHS	=	Left Hand Side
h_{beam}	=	Original beam height
h^*_{beam}	=	Adjusted beam height
t_{beam}	=	Beam thickness
ℓ_{beam}	=	Beam length
E	=	Young's modulus

[1] Aerospace Engineer, NASA Ames Systems Analysis Office, AIAA Member
[2] Aerospace Engineer, NASA Ames Systems Analysis Office, AIAA Senior Member
[3] Aerospace Engineer, NASA Ames Systems Analysis Office, AIAA Senior Member
[4] Aerospace Engineer, NASA Ames Associate

G	=	Shear modulus
ρ	=	Density
E_{beam}	=	Original beam young's modulus
G_{beam}	=	Original beam shear modulus
ρ_{beam}	=	Original beam density
E^*_{beam}	=	Adjusted beam Young's modulus
G^*_{beam}	=	Adjusted beam shear modulus
ρ^*_{beam}	=	Adjusted beam density
1-D	=	1-Dimensional
3-D	=	3-Dimensional
v	=	Poisson's ratio
g	=	Gravitational force
FR	=	Fineness Ratio
SR	=	Span Ratio
A_{CB}	=	Center body planform area
b_{CB}	=	Center body span
ℓ_{CB}	=	Center body length
θ_{CB}	=	Center body leading edge sweep
b	=	Full aircraft span
$\ell_{CB_{rect}}$	=	Center body rectangle length
ℓ_{tri}	=	Center body triangle length
OpenVSP	=	Open Vehicle Synthesis Program
PAX	=	Passenger count
c	=	Wing chord
L_{CB}	=	Center body lift
ΔP	=	Pressure differential
y	=	Span location
k	=	Constant pressure constant
b_{ow}	=	Outer wing span
L_{OW}	=	Outer wing lift
L_0	=	Lift constant
V_{OW}	=	Shear at outer wing root
$M_{B_{OW}}$	=	Bending moment at outer wing root
w_{struct}	=	Structural center body weight
A	=	A matrix of linear regression
A^T	=	Transpose of A matrix
$\vec{x}$	=	Coefficient vector of linear regression
$\vec{b}$	=	Vector of linear regression
$\rho_{f_{pass}}$	=	Passenger floor density
$t_{f_{pass}}$	=	Passenger floor thickness
$w_{f_{pass}}$	=	Passenger floor weight
$w_{f_{cargo}}$	=	Cargo floor weight
f_{con}	=	Cargo floor contour factor
$\rho_{f_{cargo}}$	=	Cargo floor density
$t_{f_{cargo}}$	=	Cargo floor thickness
k_{anchor}	=	Anchoring factor
k_{no}	=	Non-optimum factor

II. Introduction

The Blended Wing Body (BWB) represents a radical departure from conventional aircraft design, promising greater aerodynamic and structural efficiency. Unlike a conventional Tube and Wing (T&W) aircraft, with distinct fuselage and wing structures, the BWB integrates these two structures into a single, unified body. The unified body acts as an airfoil, and thus, can be analyzed with airfoil theory unlike a conventional T&W. This concept has been popularized by the likes of Liebeck, who have reported on potential weight and fuel burn benefits of the BWB when compared to a T&W [1]. These advantages, however, represent only a subset of the potential benefits of a BWB configuration: there is a significant reduction in community noise and hazard from rotor bursts, improved stall characteristics, and faster emergency egress capabilities [2].

The center body of the BWB is unique, as it is a non-circular pressure vessel that requires advanced composites technologies such as Pultruded Rod Stitched Efficient Unitized Structure (PRSEUS) to avoid structural failure and weight penalties imposed by both in- and out-of-plane loading [3]. Due to the relatively new nature of the BWB concept, historical and empirical data does not exist for conceptual aircraft designers to develop Mass Estimation Relationships (MERs), especially for estimating weights for the BWB pressurized center body. This results in the need to run computationally intensive high-fidelity methods, such as Finite Element Analysis (FEA), to obtain more accurate weights of novel BWB configurations. Bradley was the first to create a MER for a BWB pressurized cabin center-body using conventional skin-stringer structural panels based on FEA for a combination of cabin area and Take-Off Gross Weight (TOGW) [4]. An independent analysis was performed by Gern who created a program called HCDstruct, which allowed for the rapid building of BWB Finite Element Models (FEM) that could then be optimized using Nastran. Using HCDstruct, an optimized BWB model was compared against Boeing reported data and showed good agreement [5]. Another independent analysis was performed by Laughlin, who created a modeling and simulation environment that could be used for multidisciplinary analysis and weight optimization of a BWB. Trade studies performed using this environment compared predicted center body weights with passenger count for a given BWB using Bradley, Gern, and Laughlin independent methods. The results of the trade studies showed non-linearity in center body weight once a passenger count of 300 was reached as well as the advantages of a higher bay count BWB for greater than 300 passengers [6].

This paper describes the development of novel generalized parametric MER based on high fidelity FEA using PRSEUS panels for estimating the weight of a BWB pressurized cabin structure that includes cabin area, center body sweep, fineness ratio, TOGW, and span ratio. Inclusion of five parametric design variables results in a modern PRSEUS based BWB center body MER which can be used for a wide range of BWB geometries in conceptual design, sizing, and mission analysis.

III. Definition of Parameters

The definition of the center body is shown in Figure 1. The planform area (A_{CB}) of the cabin is calculated from Figure 1 by calculating the area of the triangle and rectangle comprised by the center body. Fineness ratio (FR) is defined as the ratio of center body width (b_{CB}) to length (ℓ_{CB}) as shown in Eq. (1). Center body sweep (θ_{CB}) is defined by the angle created by the leading edge of the cabin. Span ratio (SR) is defined as the ratio of b_{CB} to total aircraft span (b) as shown in Eq. (2). TOGW is calculated for each area variation based on a wing loading from 80 to 250 $\frac{lb}{ft^2}$.

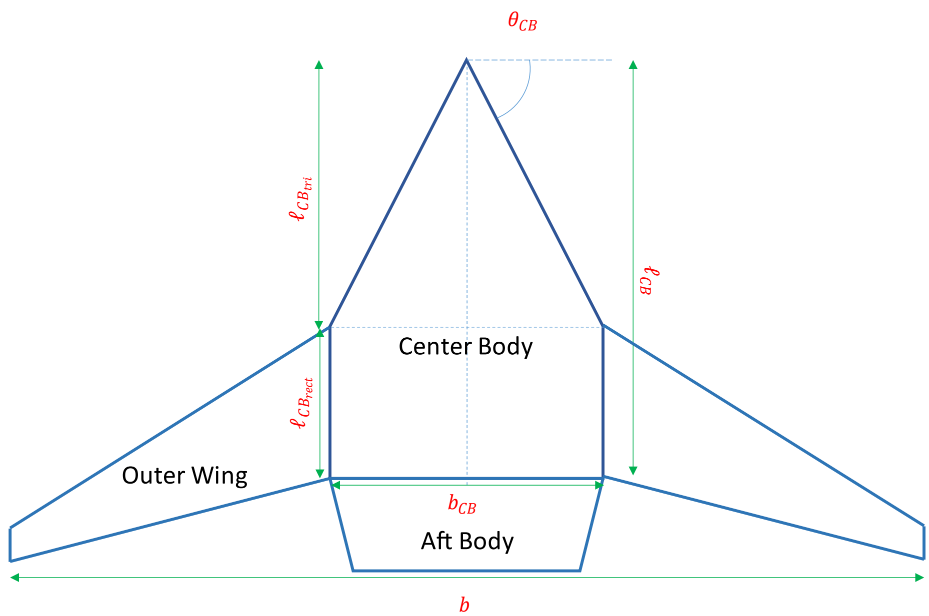

Figure 1: BWB Section Definitions

$$FR = \frac{b_{CB}}{\ell_{CB}} \tag{1}$$

$$SR = \frac{b_{CB}}{b} \tag{2}$$

It was necessary to develop a parameterized definition of the center body to enable parametric variations. The method fully defines the center body parameters $\ell_{CB}, \ell_{CB_{rect}}$, and b_{CB} in terms of A_{CB}, FR, and θ_{CB}. To define this method, the center body can be split into a triangle and rectangle shown in Figure 2**.**

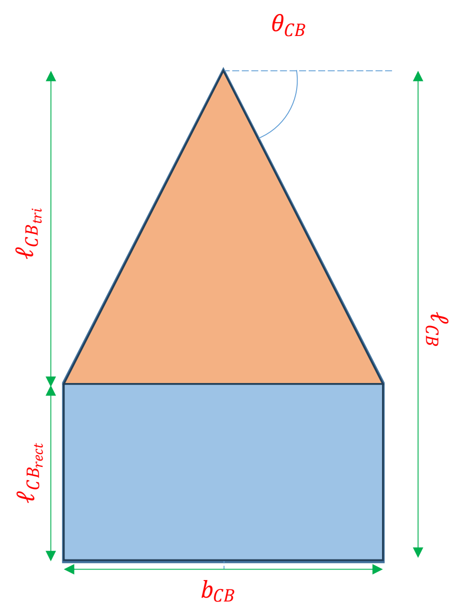

Figure 2: Sectioned center body

The total planform area can be defined as a summation of the section areas.

$$A_{CB} = b_{CB}\ell_{CB_{rect}} + \frac{1}{2}b_{CB}\ell_{CB_{tri}} \tag{3}$$

The terms in Eq. (3) are defined as,

$$b_{CB} = FR\ell_{CB} \tag{4}$$

$$\ell_{CB_{tri}} = \frac{b_{CB}}{2}\tan(\theta_{CB}) = \frac{FR\ell_{CB}}{2}\tan(\theta_{CB}) \tag{5}$$

$$\ell_{CB_{rect}} = \ell_{CB} - \ell_{CB_{tri}} = \ell_{CB} - \frac{FR\ell_{CB}}{2}\tan(\theta_{CB}) \tag{6}$$

From this, b_{CB} and $\ell_{CB_{rect}}$ have been defined in Eqs. (4) and (6). However, b_{CB} and $\ell_{CB_{rect}}$ are still in terms of the final parameter, ℓ_{CB}. Substituting Eqs. (4), (5), and (6) into Eq. (3) solves for ℓ_{CB}.

$$\ell_{CB} = \sqrt{\frac{A_{CB}}{FR(1 - \frac{1}{2}FR\tan(\theta_{CB}) + \frac{1}{4}FR\tan(\theta_{CB}))}} \tag{7}$$

IV. Improvements in Pressurized Cabin Weight Estimation

PRSEUS is a type of stitched composite that includes a pultruded rod for added bending stiffness. The additional stiffness is vital for the multiple load conditions (aerodynamic loads, internal pressure loads, maneuver loads) that the center body experiences [6]. A PRSEUS panel consists of skin, frames, and stringers as shown in Figure 3. PRSEUS frames and stringers are modeled in the FEM, enabling the creation of a MER that inherently considers the benefits of PRSEUS for all variations.

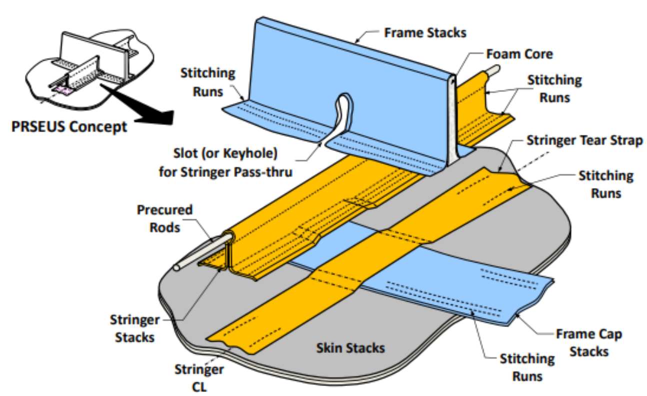

Figure 3: PRSEUS frame and stringer layout [7]

The addition of θ_{CB}, SR, and FR to the MER allows for increased sensitivity to design changes and reduces the uncertainty in the estimated values of pressurized center body weights. Modeling uncertainty reduction is especially important for BWB design, as the fuel burn advantages over a conventional T&W design are significantly penalized by only a marginal empty weight increase of 10% [8]. The Joseph 2024 MER detailed in this paper can be implemented in currently used aircraft synthesis programs, including the General Aviation Synthesis Program (GASP), Flight Optimization System (FLOPS), and Aviary, as well as be used for conceptual design, sizing, and mission analysis of BWB concept aircraft with a higher degree of specificity and reduced modelling uncertainty.

V. Procedure

A. Parametric Variations

A total of 1,296 parametric variations were created using OpenVSP [9]. Python scripts were used to prepare the input file created by OpenVSP for use in Calculix, an open-source finite element program [10]. A_{CB} has five variations, whereas θ_{CB}, FR, and SR have three variations, as shown in Table 1. TOGW has eight variations for each variation of A_{CB}, as shown in Table 2.

Table 1: Variations of cabin area, center body sweep, and fineness ratio

Parameter						
A_{CB} [ft^2]	1,750	2,000	2,200	3,000	4,250	5,500
θ_{CB} [°]	50	60	65	-	-	-
FR	0.46	0.5	0.6	-	-	-
SR	0.2	0.25	0.3	-	-	-

Table 2: Variations of TOGW based on cabin area

	A_{CB} [ft^2]					
	1,750	2,000	2,200	3,000	4,250	5,500
TOGW [lbf]	140,000	160,000	176,000	240,000	340,000	440,000
	163,333	186,666	205,333	280,000	484,500	513,333
	186,666	213,333	234,666	320,000	556,750	586,666
	210,000	240,000	264,000	360,000	629,000	660,000
	262,500	300,000	330,000	450,000	701,250	825,000
	320,833	366,666	403,333	550,000	773,500	1,008,333
	379,166	433,333	476,666	650,000	918,000	1,191,666
	437,500	500,000	550,000	775,000	1,062,500	1,375,000

B. Finite Element Model

A FEM of the center body was created based on the parameters above. FEMs of the outer wing and aft body are generally separate MERs in vehicle synthesis software and are not included in the current center body analysis for computational efficiency. Each of the parametric variation models assume centerline symmetry of the pressurized cabin of the BWB. Symmetry is used for computational efficiency, as both sides of the center body are structurally identical. Symmetric boundary conditions are used, allowing for the expansion of the center body under internal pressure at the centerline. The FEM contains two ribs and the front, rear, and side bulkheads as shown in Figure 4. These structures were modeled using Calculix S6 elements.

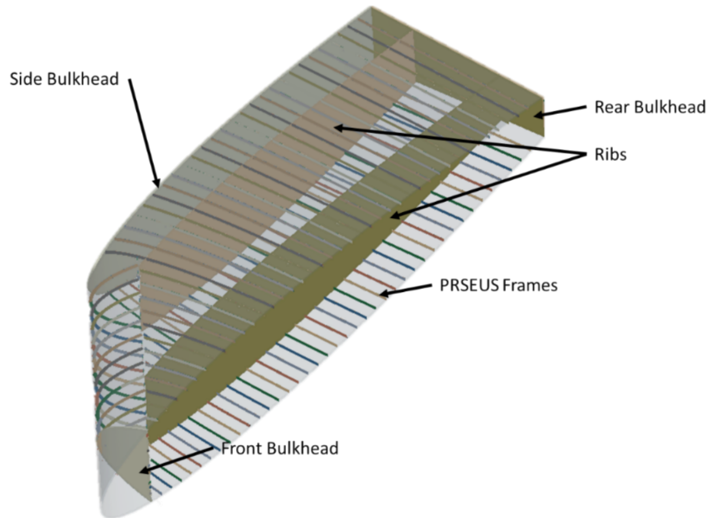

Figure 4: Structural diagram of BWB Cabin

All structures are assumed to use PRSEUS except the ribs, which are assumed to be a simple composite panel, based on Ref. [11]. PRSEUS panels used in the bulkheads are fully smeared. Doublers, cutouts, and splices are not modeled in any structures and weight contributions from these elements are included in the form of a non-optimum factor.

The resulting idealized cabin has a constant t/c of 17% as used in Ref. [4]. A 5-bay variation of the pressurized cabin was used consistently across models for simplification of model creation. A bay is defined as the location between the ribs of the center body where passengers will be seated. Gern showed no significant weight difference between 3-bay and 5-bay variations up to 300 PAX but saw significant weight reduction using 5-bays above 300 PAX [5]. Assuming 5-bays across all models enables the lowest weight estimate across all PAX ranges.

The parametric variations were built with explicitly modeled PRSEUS frames running spanwise and smeared PRSEUS stringers running chordwise on the skin. PRSEUS frames were modeled with Calculix B32 elements, shown in Figure 5, whereas PRSEUS stringers were modeled with S6 elements.

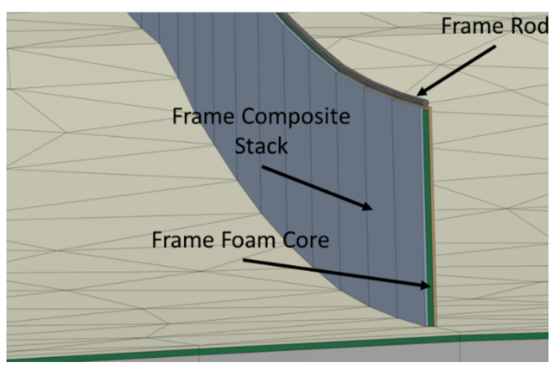

Figure 5: PRSEUS modeling in Calculix

PRSEUS frames were not modeled at full size due to curved surfaces leading to negative volumes when 1-D beam elements were expanded to 3-D elements internally in Calculix, resulting in negative Jacobians. Instead, the PRSEUS frames were smeared down to a size that would allow for explicit modeling. The smeared properties were calculated by equating flexural rigidity, torsional rigidity, and density of the full size PRSEUS frames to reduced size PRSEUS frames, as shown in Figure 6 and Eqs. (8) to (10). The length (ℓ_{beam}) of each PRSEUS frame varies between any given frame. As such, the smearing process is conducted for each PRSEUS frame independently and automatically with the use of Python.

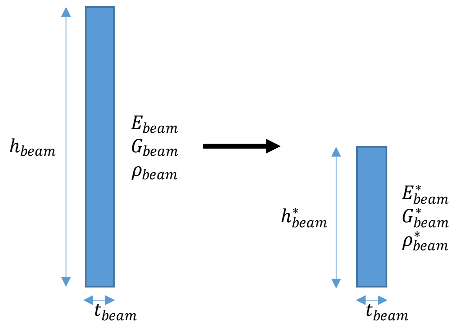

Figure 6: Smearing process for PRSEUS frames

$$E^*_{beam} = \frac{E_{beam}\, h^3_{beam}}{(h^*_{beam})^3} \tag{8}$$

$$G^*_{beam} = \frac{G_{beam}\ h_{beam}\ (h^2_{beam} + \ell^2_{beam})}{h^*_{beam}\ [(h^*_{beam})^2 + \ell^2_{beam}]} \tag{9}$$

$$\rho^*_{beam} = \frac{\rho_{beam}\, h_{beam}}{h^*_{beam}} \tag{10}$$

The spacing of the PRSEUS frames used are 24 inches and spacing of stringers are 6.0 inches [12]. Dimensions of the PRSEUS panels skin, frames, and stringers are based on Figure 3 and Figure 4 in Ref. [12]. Material properties of the IM7-8552 composite used is listed in Refs. [13, 14], shown in Table 3. A $[45/-45/0/90/45/-45/]_s$ layup is used for the tape and $[45/-45/0/45]_T$ for the fabric. Fabric composites are generally easier to mold compared to tape composites. As such, tape is assumed for the skin and ribs and fabric is assumed for the molded stringers and frames. The pultruded rod is a Toray unidirectional T800 fiber with a 3900-2B resin with properties listed in Refs. [12, 14], shown in Table 4. The foam core of the frames is Rohacell 110 WF with properties listed in Refs. [7, 12], shown in Table 5**.**

Table 3: IM7-8552 Properties [13, 14]

	E1 [msi]	E2 [msi]	ν	G12 [msi]	G13 [msi]	G23 [msi]	$\rho\ [\frac{lb}{ft^3}]$
Tape	21.3	1.26	0.32	0.749	0.749	0.435	0.057
Fabric	9.58	9.55	0.052	0.738	0.492	0.492	0.057

Table 4: Pultruded Rod Properties [12, 14]

	E1 [msi]	N	$\rho\ [\frac{lb}{ft^3}]$
Pultruded Rod	20.1	0.3	0.057

Table 5: Foam Core Properties [7, 12]

	E1 [msi]	G [ksi]	$\rho\ [\frac{lb}{ft^3}]$
Foam Core	0.01882	7.25	6.24

The passenger cabin floor and the cargo floor were assumed to be non-structural and were not included in the FEM. Weight contributions from the floors are included in the form of two separate MERs further in the text.

C. Loads

The critical load case of the center body is considered to be the 2x internal pressure load case, as internal pressure applied to a non-circular pressure vessel causes large out-of-plane loading. The base internal pressure is chosen to be 10 psi with the 2x internal pressure being 20 psi [12]. This loading was applied to the skin and bulkheads of the center body.

In addition to the internal pressure load case, a 2.5g maneuver with a 1.5x safety factor load case was included in the model. Similar to Ref. [4], a triangular lift distribution was calculated for each variation and applied to the top skin of the center body. Pressures for each skin element were calculated as a function of TOGW, b_{CB}, and chord (c). It was assumed the center body was responsible for one third of the lift of the entire aircraft [1] and the pressure at a given span location was constant across the chord at the span location. Lift (L_{CB}) across a wing can be defined in two ways: assuming lift equals weight, as shown in Eq. (11), and integration across the span shown in Eq. (12).

$$L_{CB} = \frac{TOGW}{3} \tag{11}$$

$$L_{CB} = \int_{-y}^{+y} [\Delta Pc(y)]\, dy \tag{12}$$

Equating Eqs. (11) and (12) and applying the assumption of constant pressure across the chord of a span location,

$$\int_{-y}^{+y} [\Delta Pc(y)]\, dy = \frac{TOGW}{3} \tag{13}$$

$$k = \Delta Pc(y) \tag{14}$$

Equating and simplifying,

$$\int_{-y}^{+y} [\left(\frac{k}{c(y)}\right) c(y)]\, dy = \frac{TOGW}{3} \tag{15}$$

$$k \int_{-y}^{+y} dy = \frac{TOGW}{3} \tag{16}$$

Simplifying the integral results in defining b_{CB} and can be substituted into the definition of the constant k and solved for ΔP at a given span location.

$$kb_{CB} = \frac{TOGW}{3} \tag{17}$$

$$k = \frac{TOGW}{3b_{CB}} \tag{18}$$

$$\Delta P = \frac{k}{c(y)} \tag{19}$$

ΔP is calculated for each element in the FEM dependent on the chord at the centroid of each element, then multiplied by 2.5 and 1.5 to account for the safety factor considering the maneuver load case.

An example pressure distribution, at a chord-wise location of 35 foot, across the top of the center body with a 160,000 lbf TOGW, 88-foot root chord, 57-foot tip chord, and 17.5 foot center body half span is shown in Figure 7.

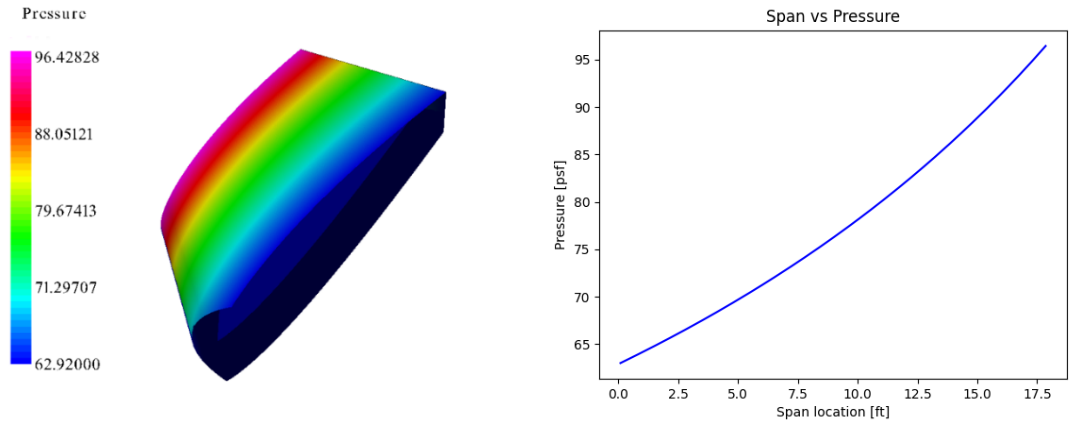

Figure 7: Example of top skin of center body with triangular lift distribution applied

The method described above, however, only considers lift created by the center body. The outer wings will generate the remaining two-thirds of the total lift where the resultant loading will be transferred to the center body. Due to the outer wing exclusion from the FEM, aerodynamic pressures were not directly applied in the same manner as the center body. Instead, the shear and moment created by the outer wing at the center body-outer wing junction is approximated by assuming an elliptical lift distribution on the outer wing, as shown in Figure 8**.** It is important to note since the center body accounts for one third of the total lift, each of the outer wings will contribute an additional third of the total lift.

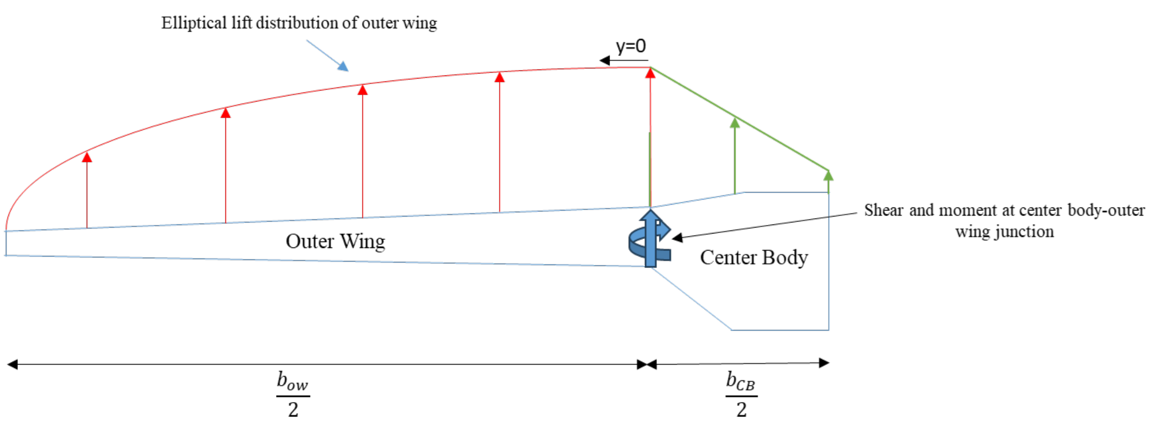

Figure 8: Approximated lift distribution of outer wing including resultant shear and moment at center body-outer wing junction

Eqs. (20), (21), and (22) were used to calculate the shear and moment at the root of the outer wing, where L_0 is a constant, b_{ow} is the span of the outer wing, and y is the span location. The span location of the center body-outer wing junction is considered $y = 0$ for the calculations as the shear and moment at the root of the outer wing is the objective.

$$L_{OW} = \int_0^{\frac{b_{ow}}{2}} L_0 \sqrt{1 - \left(\frac{2y}{\mathrm{b_{ow}}}\right)^2} \tag{20}$$

$$V_{OW} = \int_0^{\frac{b_{ow}}{2}} L_{OW}\, dy \tag{21}$$

$$M_{B_{OW}} = \int_0^{\frac{b_{ow}}{2}} y L_{OW}\, dy \tag{22}$$

Solving the integral in Eq. (20) and continuing the assumption that a single outer wing creates one third of the total lift, the constant L_0 is solved for.

$$L_{OW} = \frac{L_0 \pi b_{ow}}{8} = \frac{TOGW}{3} \tag{23}$$

$$L_0 = \frac{8TOGW}{3\pi b_{ow}} \tag{24}$$

Solving the remaining integrals in Eqs. (21) and (22) yields the shear and moment transferred to the center body. Additionally, b_{ow} can be defined in terms of b_{CB} and SR.

$$V_{OW} = \frac{TOGW}{3} \tag{25}$$

$$M_{B_{OW}} = \frac{1}{12} L_0 b_{ow}^2 \tag{26}$$

$$b_{ow} = b_{CB}(1 - SR) \tag{27}$$

The moment and shear are then multiplied by 2.5 and 1.5 to account for the maneuver load case with safety factor. To apply moment and shear to the FEM, a rigid body constraint is used with a reference node located at the centroid of the center body-outer wing junction and rigid body nodes located on the skin and rear bulkhead as shown in Figure 9. Shear is applied as a force in the z-direction and moment is applied about the x-axis.

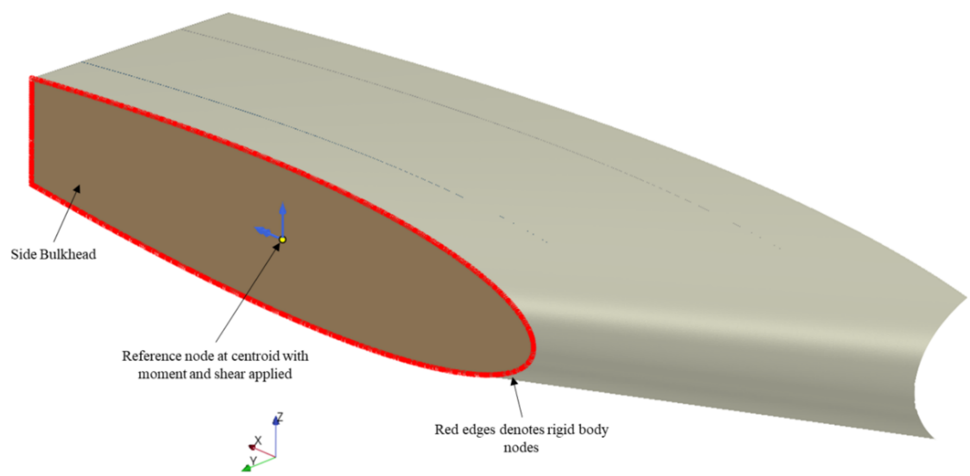

Figure 9: Shear and moment applied to center body-outer wing junction using rigid body constraint

D. Sizing Methodology for PRSEUS Center Body Structure

To reduce computational time due to the large number of models, a single design variable was considered and was selected to have the greatest impact on stiffness. The height of the PRSEUS frames was chosen as this variable as height is set to the third power in the moment of inertia equation for a rectangle. The sizing of the center body thus involved modifying the heights of the PRSEUS frames to meet strain constraints of -0.0048 to $0.0059\ \mu\frac{in}{in}$ determined in Ref. [12]. PRSEUS frame spacing and PRSEUS stringer dimensions and spacing were kept constant.

Although the PRSEUS frames were modeled explicitly, the frames were smeared to a shorter height. In a similar manner, modification of the height of the PRSEUS frames did not involve changing the physical height of the PRSEUS frames, but rather the change of physical height was reflected in a change in material properties.

Python code was created to determine the maximum strain on each individual PRSEUS frame and size individual frames based on the maximum allowable strain to maximum observed strain ratio. After sizing, the model was rerun through the process until convergence of weight was achieved.

E. Regression using FEA Data

Linear regression was used to find the best fit to the data. The linear regression method involves taking the logarithm of A_{CB}, θ_{CB}, FR, $TOGW$, SR, and sized structural weight (w_{struct}). This creates an A matrix on the LHS of size Nx5 and a B matrix on the RHS of size Nx1. Multiplying both sides by the transpose of the A matrix yields a 5x5 matrix on the LHS and a 5x1 on the RHS. These matrices can be solved to find the five constants. The process is outlined below from Eqs. (28) to (31).

$$w_{struct} = aA_{CB}^{b}TOGW^{c}FR^{d}\theta_{CB}^{e}SR^{f} \tag{28}$$

$$ln(w_{struct}) = ln(a) + bln(A_{CB}) + cln(TOGW) + dln(FR) + eln(\theta_{CB}) + fln\,(SR) \tag{29}$$

$$\begin{bmatrix} 1 & ln(A_{CB_1}) & ln(TOGW_1) & ln(FR_1) & ln(\theta_{CB_1}) & ln(SR_1) \\ 1 & ln(A_{CB_2}) & ln(TOGW_2) & ln(FR_2) & ln(\theta_{CB_2}) & ln(SR_2) \\ \vdots & \vdots & \vdots & \vdots & \vdots & \vdots \\ 1 & ln(A_{CB_N}) & ln(TOGW_N) & ln(FR_N) & ln(\theta_{CB_N}) & ln(SR_N) \end{bmatrix} \begin{bmatrix} ln(a) \\ b \\ c \\ d \\ e \\ f \end{bmatrix} = \begin{bmatrix} w_{struct_1} \\ w_{struct_2} \\ \vdots \\ w_{struct_N} \end{bmatrix} \tag{30}$$

$$\mathrm{A^T A}\vec{\mathrm{x}} = \mathrm{A^T}\vec{\mathrm{b}} \tag{31}$$

The result of fitting the FEA data using linear regression is shown in Table 6.

Table 6: Regression coefficients of MER parameters

Related Parameter	Coefficient	Linear
-	a	105.95
A_{CB}	b	0.97
$TOGW$	c	0.0021
FR	d	-0.75
θ_{CB}	e	-0.62
SR	f	-0.0008

F. Center Body Passenger Cabin and Cargo Bay Floor MERs

The passenger cabin and cargo bay floors of the center body were not modeled in the FEM as they were not considered structural members. Instead, two additional MERs were created to account for the weight contribution. The passenger cabin floor MER is based on A_{CB}, density of the floor ($\rho_{f_{pass}}$), and the thickness of the floor ($t_{f_{pass}}$). An aluminum honeycomb core with composite faces was assumed for the floor [4]. Material properties of the composite faces remain the same as the fabric used for the PRSEUS frames and stringers. The material properties used for the aluminum honeycomb core was found in Ref. [4].

$$w_{f_{pass}} = A_{CB}\rho_{f_{pass}}t_{f_{pass}} \tag{32}$$

The cargo bay floor MER is identical to that of the passenger floor MER, except for the addition of a contour factor (f_{con}), to account for the curved surface of the cargo bay floor. Based on Ref. [7], f_{con} was estimated to be 1.06 for the specific configuration, meaning the cargo bay floor covers 6% more area than the passenger cabin floor.

$$w_{f_{cargo}} = f_{con} A_{CB} \rho_{f_{cargo}} t_{f_{cargo}} \tag{33}$$

The total center body weight (w_{CB}) is then defined as the sum of the component weights.

$$w_{CB} = w_{struct} + w_{f_{pass}} + w_{f_{cargo}} \tag{34}$$

G. Anchoring of Results

The FEM created for each of the parametric variations is idealized, thus the sized FEM weight will likely be an underestimate as compared to a FEM with greater detail. As such, an anchoring factor, k_{anchor}, was required to anchor the sized FEM weights to a detailed FEM. The detailed FEM chosen was referenced from Velicki's paper, which reported a PRSEUS based center body structural FEM weight of 32,433 lbf [7]. Estimation of the geometric parameters of Velicki's model resulted in an A_{CB} of 2200 ft^2, θ_{CB} of 65°, FR of 0.46, SR of 0.28, and TOGW of 408,700 lbf. Eq. (34) was used to estimate the center body weight. The anchoring factor was then calculated by comparing the W_{CB} to the anchor weight from Velicki with results shown in Table 7.

Table 7: Anchoring of linear regression to Velicki's center body weight of 32,433 lbf

Joseph 2024 MER [lbf]	Velicki [lbf]	k_{anchor}
30,481	32,433	1.06

The value by Velicki that the regression was anchored to did not include a non-optimum factor. However the paper included a separate total non-optimum factor of ~1.15 [7], so, to be conservative, this value was rounded up to 1.20 and used as the non-optimum factor, k_{no}, included in the Joseph 2024 MER, separate from the anchoring factor. The final form of the MER can be written with the inclusion of k_{anchor} and k_{no}.

$$w_{CB} = k_{anchor} k_{no} (w_{struct} + w_{f_{pass}} + w_{f_{cargo}}) \tag{35}$$

VI. Results

The final MER to estimate the weight of the center body was created using the linear regression method and is shown in Eq. (36). The MER include a 1.2x non-optimum factor and the anchoring factor for the regression method from Table 7.

$$\boldsymbol{w_{CB} = 1.06 \cdot 1.20 \cdot [105.95(A_{CB}^{0.97})(TOGW^{0.0021})(FR^{-0.75})(\theta_{CB}^{-0.62})(SR^{-0.0008}) + w_{f_{pass}} + w_{f_{cargo}}]} \tag{36}$$

VII. Validation of Results

To validate the MER, comparisons were made to other sources that reported BWB center body weights with enough information to estimate parameters used. Gern used HCDstrut to optimize a BWB and reported a w_{CB} of 50,325 lbf with estimated A_{CB} of 3,250 ft^2, θ_{CB} of 70°, FR of 0.42, SR of 0.33 and, TOGW of 475,800 lbf. This was compared against a Boeing reported value of 51,600 lbf for a BWB with similar geometric parameters. FLOPS, an aircraft synthesis program that uses Bradley's cabin MER, was also used for comparison [5]. Table 8 shows the reference values from Ref. [5] as well as the value calculated from the Joseph 2024 MER. The MER comes within ~3% of the value reported by Boeing, shown in Table 9.

Table 8: Reference estimated cabin weights from Gern [5]

	Gern [lbf]		
Joseph 2024 MER	**FEM w/ PRSEUS**	**Boeing**	**FLOPS**
50,035	50,325	51,600	77,412

Table 9: Percent differences between Joseph 2024 MER and various Gern sources for estimated cabin weight

	Joseph 2024 MER
Gern	0.58%
Boeing	3.08%
FLOPS	42.96%

Laughlin's trade study contained estimated center body weights for BWBs ranging from 98 to 400 PAX. The study additionally reported weights estimated by Gern's method and FLOPS, which use Bradley's cabin MER [6]. The geometric parameters estimated are shown in Table 10. Estimates for Laughlin, Gern, FLOPS, and Joseph 2024 methods are plotted in Figure 10. It is important to note that Laughlin and Gern explored both 3-bay and 5-bay variations of the BWB, whereas the Joseph 2024 MER explores only the 5-bay variation. Only the 5-bay variations are plotted for all methods.

Below an A_{CB} of 3,000 ft^2, there is a good agreement for the Joseph 2024 MER with both Laughlin and Gern, whereas above an A_{CB} of 3,000 ft^2, the Joseph 2024 MER predicts lower center body weights for the given parameters. The difference in weights could be due to larger cabin areas requiring greater stiffness in ribs and bulkheads, which are not sized in the current methodology. Internal NASA systems analysis studies have shown that A_{CB} and TOGW are generally under 3500 ft^2 and 500,000 lbf, respectively, for a 450 PAX configuration.

Table 10: Geometric parameters estimated from Laughlin's trade study [6]

PAX	A_{CB} [ft^2]	θ_{CB} [°]	FR	SR	TOGW [lbf]
98	1,012.40	51.7	0.77	0.23	101,000
160	1,604.00	50.4	0.758	0.22	166,100
216	2,069.50	54.9	0.637	0.20	286,900
301	3,002.10	56	0.565	0.19	542,600
400	5,404.00	51.5	0.706	0.27	693,600

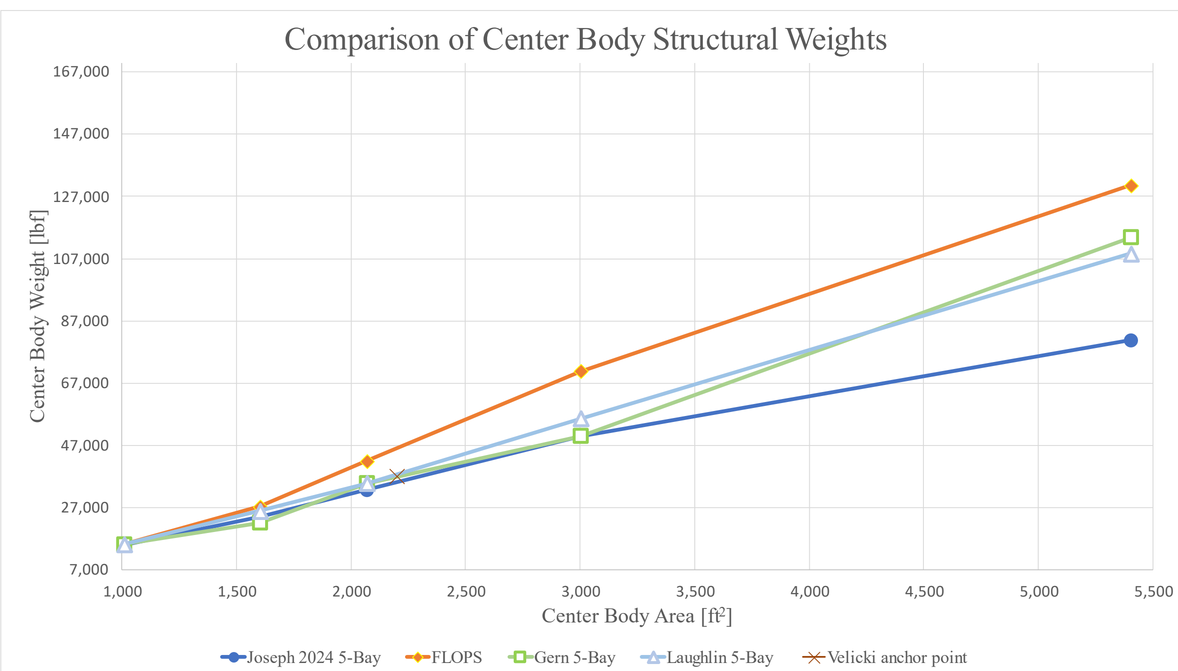

Figure 10: Comparison of center body weights for different estimation methods

VIII. Future Work

The most immediate future work to enhance the MER developed in this work would involve a sizing that includes more design variables than the height of the PRSEUS beams themselves. The number of bays could also be varied. Adding these design variables would aid in improving the trend estimation. Additionally, buckling was not addressed in this study and may affect the final cabin body weight.

IX. Conclusions

The benefits promised by the Blended-Wing-Body (BWB) concept have created a need for compact and accurate methods that are more time efficient and less computationally expensive for estimating pressurized cabin weights. The Mass Estimation Relationship (MER) presented in this paper was developed with Finite Element Methods (FEM) and anchored to a detailed advanced composite structural Finite Element Analysis (FEA). MER-estimated pressurized cabin weights compared well to other independent estimates in the literature for cabin areas smaller than 3,000 ft^2, but underpredicted the literature for larger cabin areas. The Joseph 2024 MER accounts for a greater set of vehicle parameters including cabin area, take off gross weight, sweep, span ratio, and fineness ratio to enable its use in vehicle synthesis programs to assess benefits over conventional Tube and Wing (T&W) aircraft and explore optimization of BWB aircraft.

References

[1] R. H. Liebeck, "Design of the Blended Wing Body Subsonic Transport," *JOURNAL OF AIRCRAFT,* Vols. Vol. 41, No. 1, 2004.

[2] M. A. Page, E. J. Smetak and S. L. Yang, "SINGLE-AISLE AIRLINER DISRUPTION WITH A SINGLE-DECK BLENDED-WING-BODY," *31st Congress of the Internation Council of the Aeronautical Sciences,* 2018.

[3] A. Velicki and D. Jegley, "PRSEUS Development for the Hybrid Wing Body Aircraft," *AIAA Centennial of Naval Aviation Forum "100 Years of Achievement and Progress",* 2011.

[4] K. . R. Bradley, "A Sizing Methodology for the Conceptual Design of Blended-Wing-Body Transports," *NASA/CR-2004-213016,* 2004.

[5] F. . H. Gern, "Update on HCDstruct - A Tool for Hybrid Wing Body Conceptual Design and Structural Optimization," *15th AIAA Aviation Technology, Integration, and Operations Conference,* 2015.

[6] T. W. Laughlin, J. A. Corman and D. N. Mavris, "A Parametric and Physics-Based Approach to Structural Weight Estimation of the Hybrid Wing Body Aircraft," *51st AIAA Aerospace Sciences Meeting including the New Horizons Forum and Aerospace Exposition,* 2013.

[7] A. Velicki, "Damage Arresting Composites for Shaped Phase 1 Final Report," *NASA/CR-2009-215932,* 2009.

[8] C. L. Nickol, "Hybrid Wing Body Configuration Scaling Study," *50th AIAA Aerospace Sciences Meeting including the New Horizons Forum and Aerospace Exposition,* 2012.

[9] R. A. McDonald and J. R. Gloudemans, "Open Vehicle Sketch Pad: An Open Source Parametric Geometry and Analysis Tool for Conceptual Aircraft Design," 2022.

[10] G. Dhondt and K. Wittig. [Online]. Available: https://www.dhondt.de/.

[11] A. Velicki, K. Hoffman, K. . A. Linton, J. Baraja, H.-Y. . T. Wu and P. Thrash , "Hybrid Wing Body Multi-Bay Test Article Analysis and Assembly Final Report," 2017.

[12] H.-Y. T. Wu, P. Shaw and A. Przekop, "Analysis of a Hybrid Wing Body Center Section Test Article," *54th AIAA/ASME/ASCE/AHS/ASC Structures, Structural Dynamics, and Materials Conference,* 2013.

[13] C. Kosztowny, C. Davila, K. Song, C. Rose and W. Jackson, "Experimental and numerical analysis of skin-stiffener separation using a seven point bend configuration," *AIAA Scitech 2019 Forum,* 2019.

[14] D. Jegley, "Applying a Stitched, Rod-Stiffened Concept to Heavily Loaded Structure".